



# Localization of Cesium on Montmorillonite Surface Investigated by Frequency Modulation Atomic Force Microscopy

Araki, Yuki  
Sato, Hisao  
Okumura, Masahiko  
Onishi, Hiroshi

---

**(Citation)**

Surface Science, 665:32-36

**(Issue Date)**

2017-11

**(Resource Type)**

journal article

**(Version)**

Accepted Manuscript

**(Rights)**

© 2017 Elsevier.

This manuscript version is made available under the CC-BY-NC-ND 4.0 license  
<http://creativecommons.org/licenses/by-nc-nd/4.0/>

**(URL)**

<https://hdl.handle.net/20.500.14094/90006514>



**1    Localization   of   cesium   on   montmorillonite   surface**  
**2    investigated   by   frequency   modulation   atomic   force**  
**3    microscopy**

4    Yuki Araki<sup>a,\*</sup>

5    Corresponding author

6    Email: yukiaraki@piezo.kuee.kyoto-u.ac.jp

7    TEL: +81 75 383 2307

8    FAX: +81 75 383 2308

9  
10    Hisao Satoh<sup>b</sup>

11    Email: hsatoh@mmc.co.jp

12  
13    Masahiko Okumura<sup>c</sup>

14    Email: okumura.masahiko@jaea.go.jp

15  
16    Hiroshi Onishi<sup>a</sup>

17    Email: oni@kobe-u.ac.jp

18  
19

20 (Institutional addresses)

21 <sup>a</sup> Department of Chemistry, School of Science, Kobe University, Rokkodai, Nada, Kobe,

22 Hyogo, 657-8501, Japan

23 <sup>b</sup> Mitsubishi Materials Corporation, 1002-14 Mukoyama, Naka, Ibaraki, 311-0102, Japan

24 <sup>c</sup> Center for Computational Science & e-Systems, Japan Atomic Energy Agency, 178-4

25 Wakashiba, Kashiwa, Chiba, 277-0871, Japan

26

27 \*present address

28 Department of Electronic Science and Engineering, Kyoto University, Katsura, Nishikyo,

29 Kyoto, 615-8510, Japan

30

31

32

33

34

35

36

## ABSTRACT

Cation exchange of clay mineral is typically analyzed without microscopic study of the clay surfaces. In order to reveal the distribution of exchangeable cations at the clay surface, we performed *in situ* atomic-scale observations of the surface changes in Na-rich montmorillonite due to exchange with Cs cations using frequency modulation atomic force microscopy (FM-AFM). Lines of protrusion were observed on the surface in aqueous CsCl solution. The amount of Cs of the montmorillonite particles analyzed by energy dispersive X-ray spectrometry was consistent with the ratio of the number of linear protrusions to all protrusions in the FM-AFM images. The results showed that the protrusions represent adsorbed Cs cations. The images indicated that Cs cations at the surface were immobile, and their occupancy remained constant at 10% of the cation sites at the surface with different immersion times in the CsCl solution. This suggests that the mobility and the number of Cs cations at the surface are controlled by the permanent charge of montmorillonite; however, the Cs distribution at the surface is independent of the charge distribution of the inner silicate layer. Our atomic-scale observations demonstrate that surface cations are distributed in different ways in montmorillonite and mica.

**Keywords:** montmorillonite; frequency modulation atomic force microscopy; ion exchange; adsorption

## 1. Introduction

Cations present at the surfaces and interfaces of clay minerals are exchangeable with other cations in solution to compensate the permanent negative charge of clay. Several stoichiometric investigations have revealed that the tendency for ion exchange depends on the atomic weight and electric charge. Ions that are heavier and have larger electric charge adsorb on the clay surfaces more easily than smaller ions with lower charge [1-4]. Moreover, it has been recently suggested that the hydration energy of cation affect the ion exchangeability [5]. However, as clay minerals are nm-scale particles, microscopic phenomena such as the distribution of exchangeable cations on clay surfaces and interfaces and their surface diffusion have not been clarified.

Clay minerals are phyllosilicate crystals with a 2:1 layer. Figure 1 shows the structure of montmorillonite, a type of smectite clay mineral. The monomolecular layer of the montmorillonite consists of Al-O octahedral sheet in between Si-O tetrahedral sheets. Divalent cations such as  $Mg^{2+}$  and  $Fe^{2+}$ , when substituted with  $Al^{3+}$  in the octahedral layer, produce negative charge on the montmorillonite surface. This negatively charged surface is neutralized by exchangeable cations at the surfaces and interfaces of the silicate sheets. Although the direct observation of the montmorillonite surface is difficult, the surface of muscovite mica (another 2:1 type phyllosilicate crystal and has a large flat (001) face), has

been well observed [6-9]. Through microscopic observation of the muscovite mica surfaces, several new models have been suggested for the distribution of exchangeable cations, which was previously considered to be dominated by the location of divalent cations in the silicate sheets.

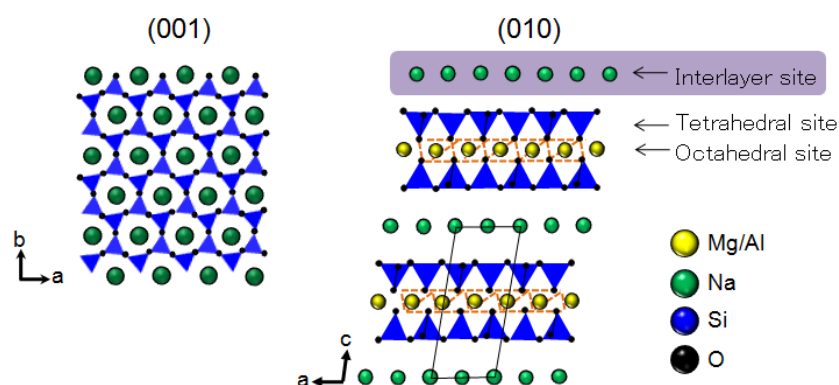


Figure 1. Crystal structure of montmorillonite. The (001) face is the basal plane of montmorillonite with six-membered rings of silicate tetrahedra. The (010) face shows the 2:1 layered structure of the clay. The green and yellow balls represent the sites of surface/interface and octahedral layer cations, respectively.

Initially, the frayed edge model was suggested, which indicates the exchangeable cations are incorporated into the “frayed edges” of the silicate layers opened by swelling [10]. Recently, experimental evidence of the ion capture at the frayed edges have been provided [11, 12]. However, this model is limited to the adsorption of the large cations, such as cesium ions

(Cs<sup>+</sup>) when the interlayer is closed because the interlayer sites are filled with small cations (e.g., K<sup>+</sup> in muscovite mica). Thus, this model cannot be applied for montmorillonite, whose interlayer easily expands by infiltration of water.

Secondly, it has been reported that the cation distribution depends on the hydration energy through atomic-scale measurement of the muscovite surface by interface dissipation microscopy (IDM) and molecular dynamics (MD) simulation [13]. The hydration energy has been compared theoretically for the random, row or hexagonal distribution of Rb<sup>+</sup> at the muscovite surface. The calculation of hydration free energy revealed that the hexagonal distribution is more favorable than the other distributions at the muscovite surface. In experiment, the hexagonal and the row pattern of Rb<sup>+</sup> were then observed at the muscovite surface in RbCl solution using IDM. As a result, the authors explained that the surface cations distribute so as to minimize the hydration energy at the muscovite mica surface. This “water-induced correlation model” suggests that the distribution of the cations at the surface is independent of the cation distribution in the silicate sheet.

These investigations have provided several models of cation distribution in muscovite mica. However, the location of the negative charge source is different between clay and mica. In mica, divalent cations, as sources of negative charge, are located in the Si-O tetrahedral layer. However, clay holds the divalent cations in the Al-O octahedral layer. This difference is

likely to induce different behavior of the exchangeable cations.

In this study, we aimed to clarify the cation distribution on the montmorillonite surface by visualizing the montmorillonite surface structure at the atomic scale. We observed the 100 nm-scale montmorillonite surface using frequency modulation atomic force microscopy (FM-AFM), which has achieved atomic and molecular scale visualization in a liquid environment.

## **2. Material and methods**

### *2.1. Sample*

Natural montmorillonite (Tsukinuno, Japan) was used in this study. The interlayer of the montmorillonite sample was originally dominated by  $\text{Na}^+$  ions. Using chemical component analysis, we confirmed that the other exchangeable cations are rarely present in montmorillonite as described in Section 3.1.

### *2.2. Solution*

We selected  $\text{Cs}^+$  as the observable cation because large cations are most suitable for identifying the surface cations on the montmorillonite surface. Therefore, the montmorillonite surfaces were observed in a 500 mM CsCl solution (Wako, 99.0 %). The  $\text{Cs}^+$  is easily exchanged with surface  $\text{Na}^+$  of montmorillonite because of its ion exchange tendency. The exchange of  $\text{Na}^+$  and  $\text{Cs}^+$  was confirmed by the analysis of the chemical composition of



montmorillonite as described in Section 3.1.

### 2.3. FM-AFM

We employed FM-AFM to observe the surface of the 100 nm scale particles of montmorillonite with atomic resolution. In the frequency modulation mode of non-contact atomic force microscopy, the interaction force between the tip of the probe and the atoms at the sample surface was detected by the frequency shift ( $\Delta f$ ) of the cantilever oscillation. The noise was lowered, and the sensitivity for the detection of the cantilever oscillation in the liquid was improved [14]. With improved sensitivity, imaging of the surface structure with an atomic resolution was achieved [9, 15-17]. We used a microscope compatible with SPM-8000FM (Shimadzu, Japan). The probe was an Au-coated silicon cantilever (PPP-NCHAuD, Nanosensors, Switzerland). The eigen frequency of the cantilever was 155 kHz, the quality factor was approximately 8, and the spring constant was approximately 40 N/m in the CsCl solution. The FM-AFM equipment was located in an incubator (CN-40A, Mitsubishi Electric Engineering, Japan) to maintain the temperature at 22°C.

### 2.4. Chemical component analysis.

The chemical components of montmorillonite before and after the ion exchange were analyzed by energy dispersive X-ray spectrometry (EDS; EX-2300, JEOL, Japan) coupled with a field emission-scanning electron microscope (FE-SEM; JSM-6700F, JEOL, Japan) and

a field emission transmission electron microscope (FE-TEM; JEM-2100F, JEOL, Japan). The FE-SEM/EDS can analyze all the chemical components of the aggregated montmorillonite blocks. Therefore, it was used to confirm the ratio of  $\text{Na}^+$  in naturally occurring montmorillonite. In contrast, the FE-TEM/EDS was applied to analyze the components of a thin montmorillonite particle with a few silicate layers to ensure comparability to the FM-AFM measurement of the montmorillonite surface. The natural montmorillonite block was immersed in purified water for dispersion of montmorillonite by swelling. Next, a drop of the dispersed liquid was loaded and dried on a highly oriented pyrolytic graphite (HOPG) substrate. The remaining dispersed liquid was exchanged with CsCl solution for ion exchange. The montmorillonite particles were then immersed in CsCl solution for 2 h. To avoid precipitation of CsCl salt, the exchanged montmorillonite particles were immersed in ethanol and then loaded on the HOPG substrate for EDS measurement. Note that the montmorillonite particles for FM-AFM observation and those for chemical measurement by EDS were from different blocks, though they were sourced from the same montmorillonite rock.

## *2.5. FM-AFM observation procedure*

First, the dispersed liquid of natural montmorillonite was loaded on the cleaved surface of a muscovite substrate. After the montmorillonite sheets had dried, they were fixed by physisorption of the monomolecular sheets of the montmorillonite on the substrate. Next, a

100 µl droplet of CsCl solution was placed on the dried muscovite substrate along with the montmorillonite sheets. Observation of the montmorillonite surface by FM-AFM was then performed.

### 3. Results and discussion

#### 3.1. Conformation of Na-Cs exchange by EDS analysis.

The averaged chemical formula of the natural montmorillonite block was  $\text{Na}_{0.80}, \text{K}_{0.11}(\text{Mg}_{1.38}, \text{Ca}_{0.16}, \text{Fe}_{0.03}, \text{Al}_{2.54})\text{Si}_{8.08}\text{O}_{20}(\text{OH})_4$ . This shows that the surfaces and interlayers were dominated by  $\text{Na}^+$ . The averaged chemical formula of montmorillonite after immersion in CsCl solution was  $\text{Cs}_{0.42}(\text{Mg}_{0.69}, \text{Fe}_{0.12}, \text{Al}_{2.93})(\text{Si}_{7.93}, \text{Al}_{0.07})\text{O}_{20}(\text{OH})_4$ . The chemical formula of cations of tetrahedral and octahedral layers fluctuated before and after immersion in the CsCl solution because different montmorillonite particles were measured in EDS analysis before and after immersion in the CsCl solution, as mentioned in Section 2.4. The EDS analysis showed that exchangeable  $\text{Na}^+$  and some other cations at the surfaces and interlayers were completely exchanged with  $\text{Cs}^+$  after immersion in CsCl solution. According to the chemical formula of Cs-exchanged montmorillonite, the maximum ratio of  $\text{Cs}^+$  at cation sites on the surfaces is about 10%.

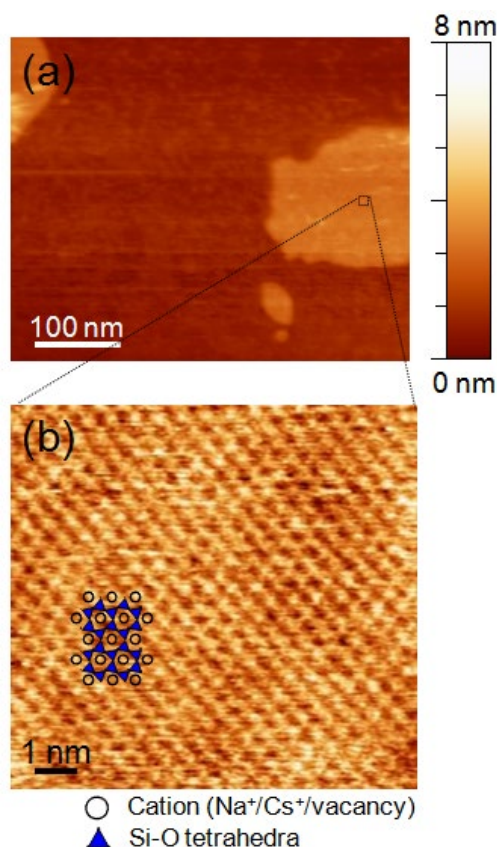
#### 3.2. Linear distribution of Cs at montmorillonite surface

The topographic images of montmorillonite surface just after the CsCl solution was

178 loaded are shown in Figure 2. Figure 2(a) shows montmorillonite particles on a mica substrate.  
179 The particle was shapeless with a size of about 100 nm and a thickness of 1 nm. Fig. 2(b)  
180 shows the montmorillonite surface at the atomic scale a few minutes after the CsCl solution  
181 was loaded. The threshold value of the frequency shift was +115 Hz and the oscillation  
182 amplitude (peak-to-peak) was approximately 1.6 nm. The contrast in topographic images  
183 reflects the interaction force between the tip of the cantilever and the surface atoms. The  
184 brighter and darker areas in the topographic image correspond to the repulsive and attractive  
185 forces of the tip, respectively. According to the chemical component analysis, about 90% of  
186 the cation sites in the silicate rings were vacant. However, all cation sites seemed to be filled  
187 in the FM-AFM images. The observation of the muscovite mica surface by FM-AFM showed  
188 two characteristic patterns: honeycomb-like and the dot-like [9]. The honeycomb-like pattern  
189 is consistent with the distribution of the six-membered ring of Si-O tetrahedral of the mica  
190 surface. In contrast, the dot-like pattern is consistent with the distribution of the closest  
191 hydrated water molecules, which are located at the center of the Si-O ring according to  
192 three-dimensional  $\Delta f$  mapping by FM-AFM and the theoretical simulation [18]. Furthermore,  
193 a few studies have reported vacancies at the center of the Si-O ring of the muscovite mica  
194 surfaces in the liquid [19]; however, these are typically observed under an ultrahigh vacuum  
195 condition [20, 21]. Therefore, it has been suggested that vacancies at the center of the

196 six-membered rings of silicate were filled with the adsorbed water in liquid. This is supported  
197 by other measurements of water distribution in the vicinity of the muscovite surfaces by X-ray  
198 reflectivity [22, 23] and theoretical simulations [24, 25]. In our images, the montmorillonite  
199 surfaces also showed a honeycomb-like pattern (Figure A.1) in addition to the dot-like pattern  
200 shown in Fig. 2(b). These surface patterns changed depending on the threshold value of  $\Delta f$ , so  
201 the surface pattern is considered to depend on the tip-sample distance as mentioned in  
202 Fukuma et al. [9]. The structure of the (001) face is similar in muscovite mica and  
203 montmorillonite, so the dot-like protrusions shown in Fig. 2(b) would represent the closest  
204 water molecules in the Si-O rings of the montmorillonite surface.

205



206  
 207 Figure 2. FM-AFM images of the montmorillonite (001) face in the 0.5 M CsCl solution. (a)  
 208 The monomolecular sheet of montmorillonite on the muscovite substrate. (b) Magnified  
 209 image of the black box (a) at the atomic scale a few minutes after the CsCl solution was added.  
 210 An illustration of the crystal structure of (001) face of the montmorillonite was layered onto  
 211 the topographic image.

212  
 213 Figure 3 shows the montmorillonite surface 4 h after the solution was added. This image was  
 214 obtained with a threshold value of +304 Hz and a peak-to-peak amplitude of 0.8 nm. The  
 215 topographic image shows a hexagonal dotted pattern. However, several linear protrusions,

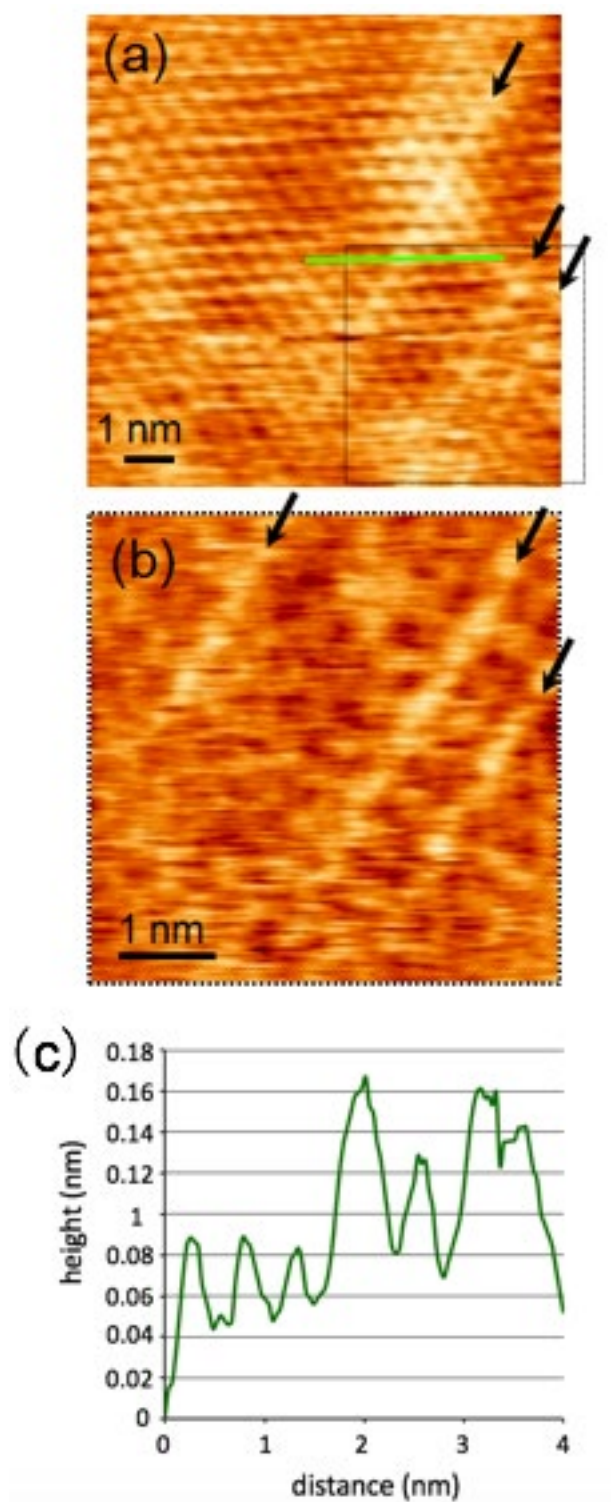
216 indicated by arrows in Figure 3(b), were observed at the montmorillonite surface. The height  
217 difference between the line protrusions and the other protrusions was 0.8 Å (Fig. 3c). Such  
218 line protrusions, distributed along the lattice line with a height difference of 0.6–1 Å, were  
219 observed reproducibly (Fig. A.2). Furthermore, line protrusions were observed in a different  
220 scan area (Fig. 3b) and scan angle (Fig. A.3), indicating that the line protrusions were not  
221 artifacts. These protrusions were observed along a single grid of the lattice, indicating that  
222 they were unlikely to be contaminated by organic molecules or salt. Figure A.4 presents  
223 sequential images before and after the line protrusions appeared on the montmorillonite  
224 surface. It is shown that the line protrusion was adsorbed in the scanning of one frame (15 s).  
225 Subsequently, these protrusions stayed in the same place for 10 min. Although the total length  
226 of the line protrusions was unknown and their period was random, the width and the number  
227 of the line protrusions did not change and thus we estimated that the adsorption was in  
228 equilibrium by 15 s.

229 The Cs<sup>+</sup> ratio to all cation sites (about 10%) at the montmorillonite surfaces indicated by the  
230 FE-TEM/EDS analysis was consistent with the ratio of the linear brighter protrusions to the  
231 other area in the topographic image of FM-AFM (Table 1). This suggests that the linear  
232 protrusions show the distribution of Cs<sup>+</sup>. A previous study of molecular dynamics simulations  
233 of the distribution of water and cations in the vicinity of mica surfaces has shown that both

234  $\text{Cs}^+$  and oxygen in water molecules are located at the same height (0.2 nm) from the silicate  
235 plane of the mica surface [25]. Therefore, FM-AFM depicts hydrated  $\text{Cs}^+$  as larger protrusions  
236 than others because hydrated  $\text{Cs}^+$  (diameter: 6.6 Å) is larger than a single water molecule ( $\approx 3$   
237 Å). Conversely, an inhomogeneous contrast of the whole montmorillonite surfaces was  
238 observed in the FM-AFM observation, irrespective of the type of surface cation (Figure A.5);  
239 however, the line protrusions were observed only in the CsCl solution. This also indicates that  
240 the line distribution of the surface cations can be visualized in case of larger cations such as  
241  $\text{Cs}^+$ . These results also support the idea that the linear protrusions represent  $\text{Cs}^+$ .

242





243

244 Figure 3. FM-AFM images of the montmorillonite (001) face 4 h after the 0.5 M CsCl

245 solution was added. (a) The linear protrusions on the montmorillonite surface. The brighter

protrusions are indicated by arrows. (b) The magnified image in the black box in (a). The linear protrusions are indicated by arrows. (c) The line profile along the green line of (a).

Table 1. Comparison of  $\text{Cs}^+$  ratios to the other cation sites on the montmorillonite surface measured by EDS and FM-AFM.

methods	Occupation of interlayer sites (%)			total (%) (A+B+C)
	(A) $\text{Cs}^+$	(B) other cations ( $\text{Na}^+$ , $\text{Ca}^{2+}$ , $\text{K}^+$ )	(C) vacancies	
FE-TEM/EDS	8.49	0.00	91.51	100.00
FM-AFM	10	90		100

### 3.3. Relation of layer charge to local distribution of Cs

The distribution of Cs at the montmorillonite surface is generally considered that the  $\text{Cs}^+$  and  $\text{Mg}^{2+}$  are located close each other to minimize Coulomb energy. However, linear distribution of inner  $\text{Mg}^{2+}$  is unstable according to the calculation of free energy, as shown in the Appendix (Fig. A.6, Table A.1 and A.2). This suggests that the distribution of exchangeable cations is independent of the  $\text{Mg}^{2+}$  distribution in the octahedral layer. This numerical result is consistent with the water-induced correlation model [13], which predicts ordered cation distribution without correlation between cations on the surface and those in the silicate sheet. However, this result does not imply that the charge distribution in the silicate

layer has no effect on the surface cations. If the surface cations were not affected by the charge distribution at the inner layer, the exchangeable cations could be diffused at the surface. However, the results indicate that surface Cs stayed stable for more than 10 min. This suggests the lower mobility of the exchangeable cations on the surface of montmorillonite as well as on that of mica. Conversely, it has been reported that the amount of adsorbed  $\text{Rb}^+$  increased with an increase in the concentration of  $\text{RbCl}$ , according to the observation of a mica surface using IDM by Ricci et al. [13]. Ricci et al. [13] also showed that the surface cation sites were completely covered with  $\text{Rb}^+$  in 10 mM  $\text{RbCl}$ . In contrast, our experiments using montmorillonite in 500 mM  $\text{CsCl}$  solution showed that the number of adsorbed  $\text{Cs}^+$  followed the ratio of  $\text{Mg}^{2+}$  in the octahedral layer, even in higher concentrations of  $\text{CsCl}$ . This demonstrates that the number of adsorbed exchangeable cations on the montmorillonite surface is strictly controlled by the amount of negative charge in the inner layers. Our results show that the permanent layer charge of montmorillonite dominates the stability and the amount of adsorption of surface cations but not their distribution.

#### **4. Conclusions**

The atomic-scale change on the surface of montmorillonite due to the exchange of ions with  $\text{Cs}^+$  was observed using FM-AFM. The change could be seen as linear protrusions in the  $\text{CsCl}$

solution. By conducting chemical component analysis using EDS, we determined that the linear protrusions represented the adsorbed  $\text{Cs}^+$ . We also identified that  $\text{Cs}^+$  was distributed in a linear pattern and confirmed that linear Cs was stable without surface diffusion and desorption. Furthermore, the ratio of Cs adsorption at the montmorillonite surface followed the chemical formula of the montmorillonite measured using EDS, even in the high-concentration CsCl solution.

This study demonstrated that the FM-AFM observation is valid for the study of ion exchange at the surface of clay nano-particles. More detailed observations using this technique are required to directly reveal the ion exchange processes occurring at the clay surfaces.

#### **Competing interests**

The authors declare that they have no competing interests.

#### **Author's contributions**

Yuki Araki proposed the topic, designed the study and carried out the experiments using FM-AFM. Hisao Satoh carried out the analysis by EDS and helped in the interpretation of data. Masahiko Okumura conducted the free energy calculation and helped in the interpretation of data. Hiroshi Onishi collaborated with Yuki Araki in writing the manuscript.

298 All authors have read and approved the final manuscript.

299

## 300 **Acknowledgements**

301 The FE-TEM/EDS measurement was supported by Professor Yuki Kimura (Institute of Low  
302 Temperature Science, Hokkaido University). The numerical calculations were performed on  
303 the ICE X supercomputer in CCSE, JAEA. This work was supported by a Grant-in-Aid for  
304 Scientific Research (B) (Grant Number 25286009). Yuki Araki was partly funded by the  
305 Advanced Technology Institute (No. RG2610).

306

## 307 **Appendix A. Supplementary data**

308 Additional observations of the montmorillonite surface and the calculation of grand state  
309 energy differences depending on the distribution of inner  $\text{Mg}^{2+}$  are supplied as supplementary  
310 data.

311

## 312 **References**

- 313 [1] Thompson, H. S., On the adsorbent power of soils. *J. R. Agric. Soc. Engl.* **11**, 68-74  
314 (1850).
- 315 [2] Way. J. T., On the power of soils to absorb manure. *J. R. Agric. Soc. Engl.* **11**, 313-379

316 (1850).

317 [3] Carroll, D., Ion Exchange in Clays and Other Minerals. *Geol. Soc. Amer. Bull.* **70**,  
318 749-780 (1959).

319 [4] Polyakov, V. E. and Tarasevich, Y. I., Ion-Exchange Equilibriums Involving  
320 Single-Charged Cations on Saponite. *J. Water Chem. Tech.* **34**, 11-16 (2012).

321 [5] Teppen, B. J. and Miller, D. M., Hydration Energy Determines Isovalent Cation  
322 Exchange Selectivity by Clay Minerals. *Soil Sci. Soc. Am. J.* **70**, 31-40 (2006).

323 [6] Sharp, T. G.; Oden, P. I.; Buseck, P. R., Lattice-scale imaging of mica and clay (001)  
324 surfaces by atomic force microscopy using net attractive forces. *Surf. Sci. Lett.*  
325 L405-L410 (1993).

326 [7] Nishimura, S.; Biggs, S.; Scales, P. J.; Healy, T. W.; Tsunematsu, K.; Tateyama, T.,  
327 Molecular-Scale Structure of the Cation Modified Muscovite Mica Basal Plane.  
328 *Langmuir* **10**, 4554-4559 (1994).

329 [8] Kuwahara, Y., Muscovite surface structure imaged by fluid contact mode AFM. *Phys.*  
330 *Chem. Minerals* **26**, 198-205 (1999).

331 [9] Fukuma, T.; Kobayashi, K.; Matsushige, K.; Yamada, H., True atomic resolution in liquid  
332 by frequency-modulation atomic force microscopy. *Appl. Phys. Lett.* **87**, 034101 (2005).

333 [10] McKinley, J. P.; Zachara, J. M.; Heald, S. M.; Dohnalkova, A.; Newville, M. G.; Sutton,

334 S. R., Microscale distribution of cesium sorbed to biotite and muscovite. *Environ. Sci.*  
 335 *Technol.* **38**, 1017-1023 (2004).

336 [11] Fuller, A. J.; Shaw, S.; Ward, M. B.; Haigh, S. J.; Mosselmans, J. F. W.; Peacock, C. L.;  
 337 Stackhouse, S.; Dent, A. J.; Trivedi, D.; Burke, I. T., Cesium incorporation and retention  
 338 in illite interlayers. *Appl. Clay Sci.* **108**, 128-134 (2015).

339 [12] Sato, K.; Fujimoto, K.; Dai, W.; Hunger, M., Quantitative Elucidation of Cs Adsorption  
 340 Sites in Clays: Toward Sophisticated Decontamination of Radioactive Cs. *J. Phys. Chem.*  
 341 *C* **120**, 1270-1274 (2016).

342 [13] Ricci, M.; Spijker, P.; Voitchovsky, K., Water-induced correlation between single ions  
 343 imaged at the solid-liquid interface. *Nat. Commun.* **5**, 5400 (2014).

344 [14] Fukuma, T.; Kimura, M.; Kobayashi, K.; Matsushige, K.; Yamada, H., Development of  
 345 low noise cantilever deflection sensor for multienvironment frequency-modulation  
 346 atomic force microscopy. *Rev. Sci. Instrum.* **76**, 053704 (2005).

347 [15] Rode, S.; Oyabu, N.; Kobayashi, K.; Yamada, H.; Kühnle, A., True atomic-resolution  
 348 imaging of (1014) calcite in aqueous solution by frequency modulation atomic force  
 349 microscopy. *Langmuir* **25**, 2850-2853 (2009).

350 [16] Imada, H.; Kimura, K.; Onishi, H., Atom-resolved AFM imaging of calcite nanoparticles  
 351 in water. *Chem. Phys.* **419**, 193-195 (2013).

- 352 [17] Ido, S.; Kimiya, H.; Kobayashi, K.; Kominami, H.; Matsushige, K.; Yamada, H.,  
353 Immunoactive two-dimensional self-assembly of monoclonal antibodies in aqueous  
354 solution revealed by atomic force microscopy. *Nature Mater.* **13**, 264-270 (2014).
- 355 [18] Kobayashi, K.; Oyabu, N.; Kimura, K.; Ido, S.; Suzuki, K.; Imai, T.; Tagami, K.;  
356 Tsukada, M.; Yamada, H., Visualization of hydration layers on muscovite mica in  
357 aqueous solution by frequency-modulation atomic force microscopy. *J. Chem. Phys.* **138**,  
358 184704 (2013).
- 359 [19] Hoogenboom, B. W.; Hug, H. J.; Pellmont, Y.; Martin, S.; Frederix, P. L. T. M.; Fotiadis,  
360 D.; Engel, A., Quantitative dynamic-mode scanning force microscopy in liquid. *Appl.*  
361 *Phys. Lett.* **88**, 193109 (2006).
- 362 [20] Sugawara, Y.; Uchihashi, T.; Abe, M.; Morita, S., True atomic resolution imaging of  
363 surface structure and surface charge on the GaAs (110). *Appl. Surf. Sci.* **140**, 371-375  
364 (1999).
- 365 [21] Morita, S.; Abe, M.; Yokoyama, K.; Sugawara, Y., Defects and their charge imaging on  
366 semiconductor surfaces by noncontact atomic force microscopy and spectroscopy. *J.*  
367 *Cryst. Growth* **210**, 408-415 (2000).
- 368 [22] Schlegel, M. L.; Nagy, K. L.; Fenter, P.; Cheng, L.; Sturchio, N. C.; Jacobsen, S. D.,  
369 Cation sorption on the muscovite (001) surface in chloride solutions using



370 high-resolution X-ray reflectivity. *Geochim. Cosmochim. Acta*, **70**, 3549-3565 (2006).  
 371 [23] Leng, Y. and Cummings, P. T., Hydration structure of water confined between mica  
 372 surfaces. *J. Chem. Phys.* **124**, 074711 (2006).  
 373 [24] Park, S. H. and Sposito, G., Structure of water adsorbed on a mica surface. *Phys. Rev.*  
 374 *Lett.* **89**, 085501 (2002).  
 375 [25] Sakuma, H. and Kawamura, K., Structure and dynamics of water on Li<sup>+</sup>-, Na<sup>+</sup>-, K<sup>+</sup>-, Cs<sup>+</sup>-,  
 376 H<sub>3</sub>O<sup>+</sup>-exchanged muscovite surfaces: A molecular dynamics study. *Geochim.*  
 377 *Cosmochim. Acta* **75**, 63-81 (2011).

## **Appendix A**

### **Table of Contents**

**Figure A.1.** Surface configurations of montmorillonite.

**Figure A.2.** Examples of line protrusion in 500 mM CsCl solution.

**Figure A.3.** Topographic images of line protrusion with changing scan angle.

**Figure A.4.** Sequential images of montmorillonite surface before and after the  
appearance of line protrusions.

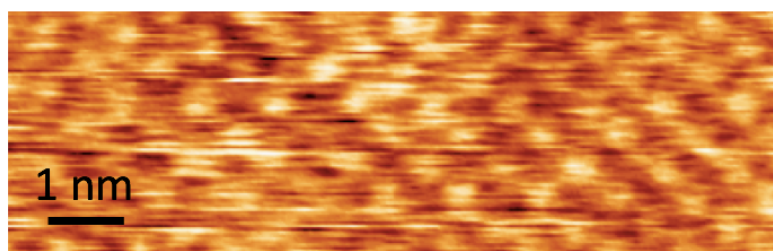
**Figure A.5.** Montmorillonite surface in the NaCl, KCl and CaCl<sub>2</sub> solutions.

**Figure A.6.** Montmorillonite slab systems.

**Table A.1.** Lattice parameters.

**Table A.2.** Relative formation energy.

dot-like pattern



honeycomb-like pattern

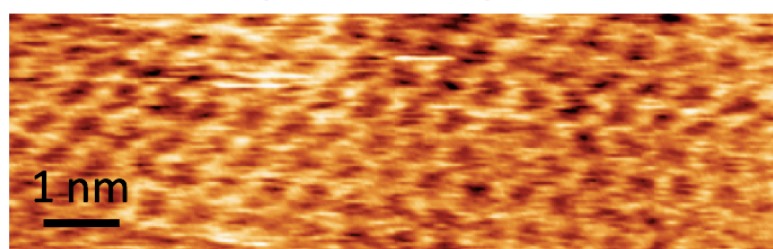


**Figure A.1.** Surface configurations of montmorillonite. Dot-like and honeycomb-like patterns were observed with  $\Delta f$  threshold value of 90 and 170 Hz and peak-to-peak amplitude of 0.8 nm and 0.4 nm, respectively. The differences in the direction of the atomic row between the upper and the lower images were due to thermal drift.

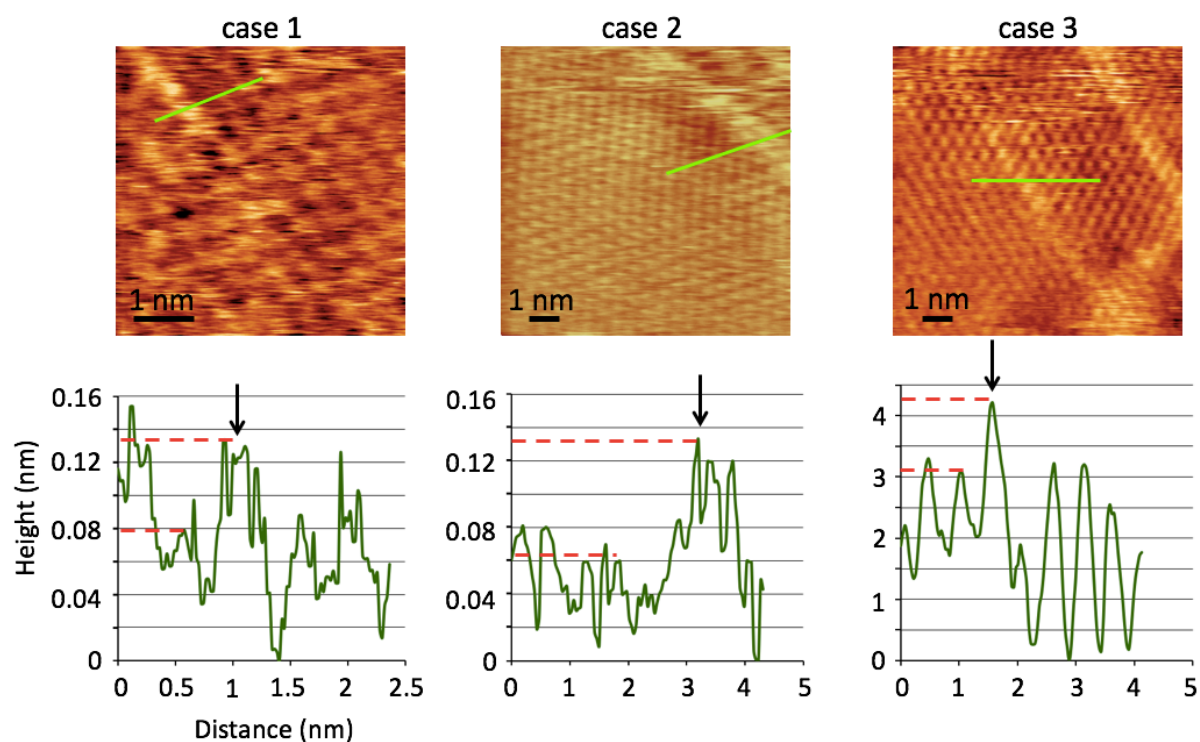


**Figure A.2.** Examples of line protrusion in 500 mM CsCl solution. Upper images show the topographic images of line protrusions which were observed in the other trials. The lower graphs represent line profiles along the green lines in the upper images. The arrows indicate the line protrusion.

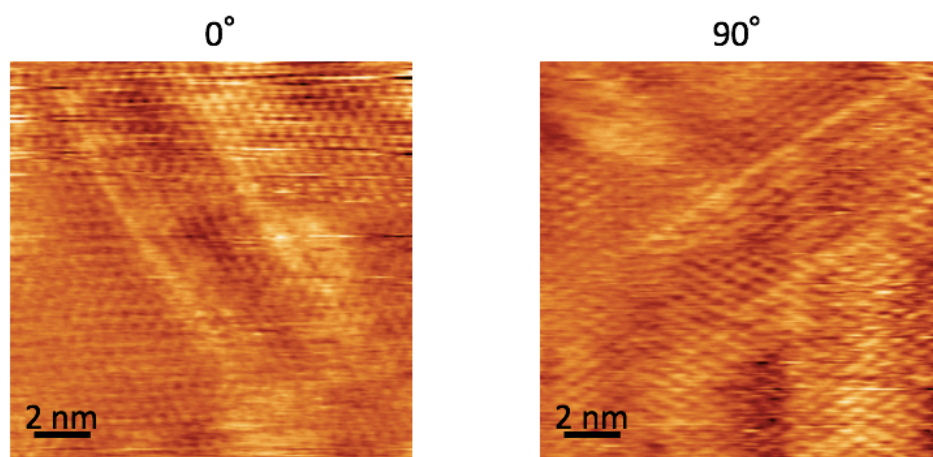


**Figure A.3.** Topographic images of line protrusion with changing scan angle. The left and right images were observed with the scan angle of  $0^\circ$  and  $90^\circ$ , respectively.

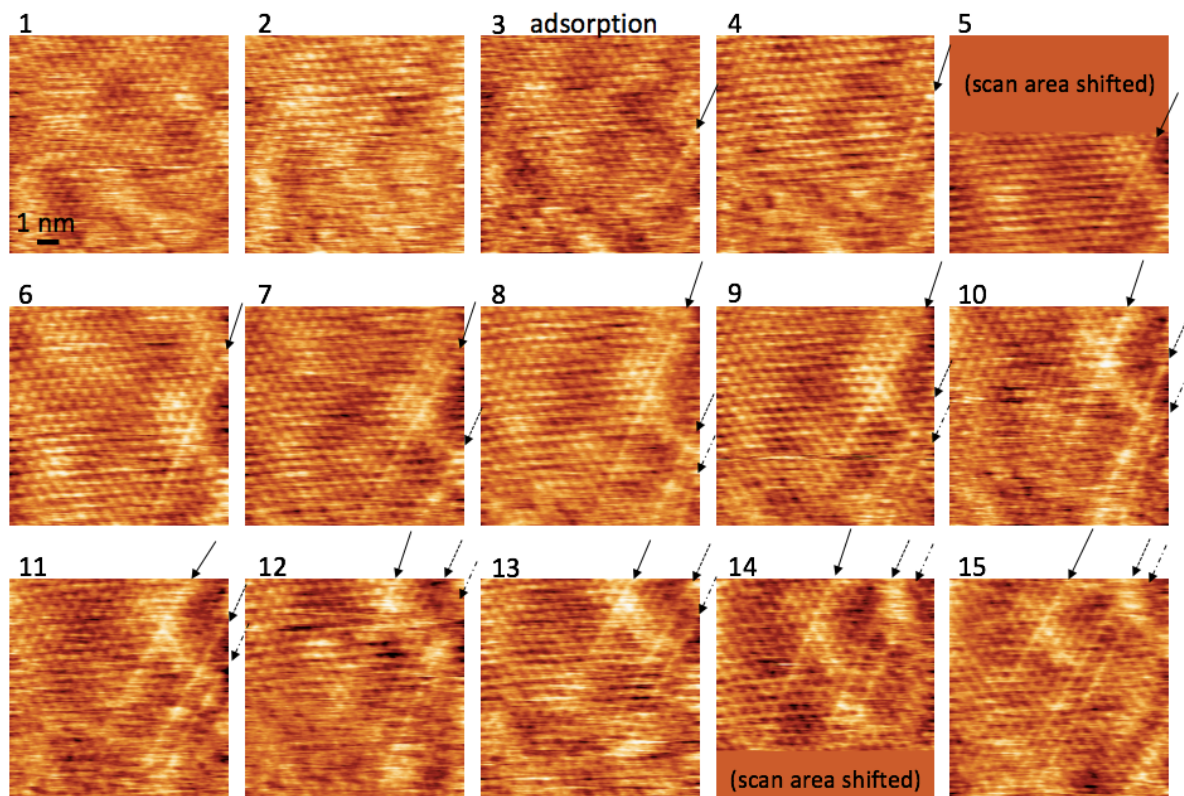


**Figure A.4.** Sequential images of the montmorillonite surface before and after the appearance of line protrusions. Frame 1 was observed in 15 s. Frame 9 is the same as Figure 3(a). The scan area was drifted to the upper left, so the area was shifted in the Frames 5 and 14. The  $\Delta f$  threshold value and the oscillation amplitude were maintained at 304 Hz and 0.8 nm<sub>p-p</sub>, respectively.

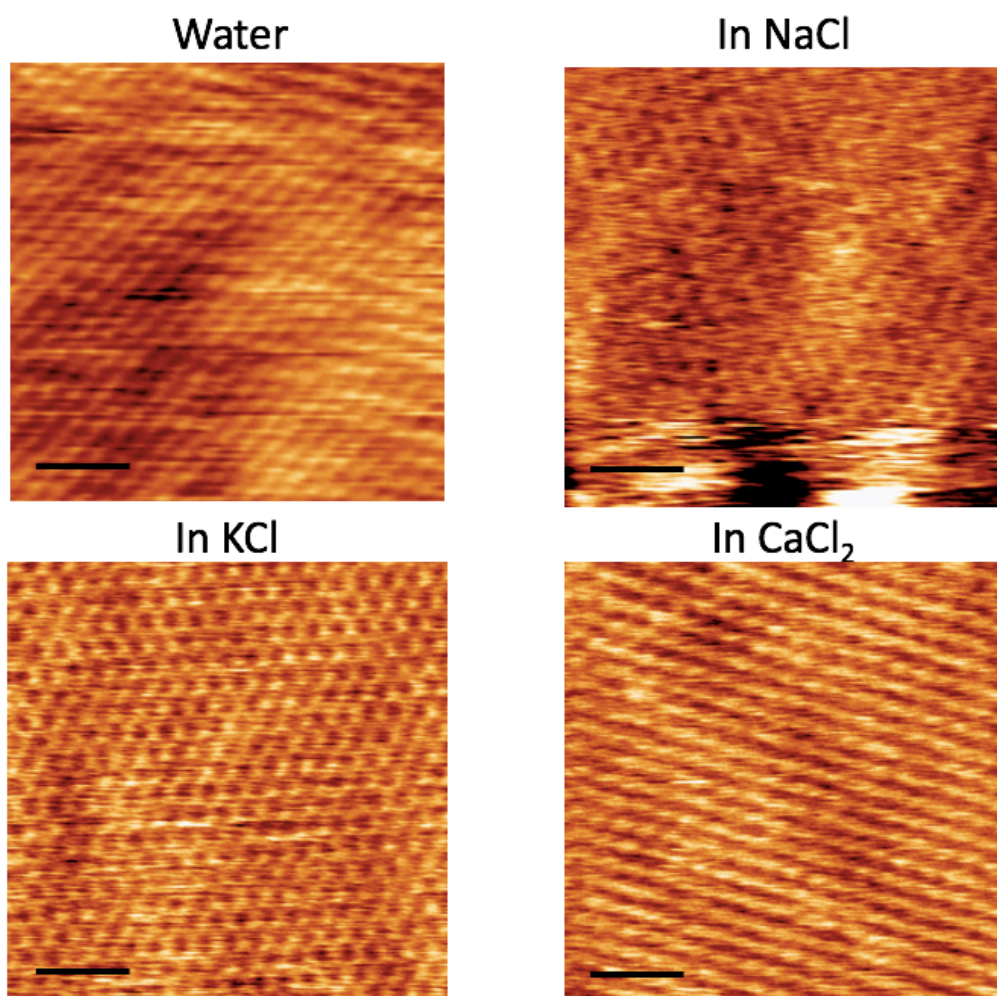


**Figure A.5.** Montmorillonite surface in the NaCl, KCl and CaCl<sub>2</sub> solutions. The topographic images of montmorillonite surface in 100 mM NaCl, KCl and CaCl<sub>2</sub> solutions were observed 4 h after the solutions were added. Scale bars indicate 2 nm.



## **The calculation of grand state energy differences depending on the distribution of inner $\text{Mg}^{2+}$**

In order to estimate how the  $\text{Mg}^{2+}$  configuration in the octahedral sheet affects the linear pattern of  $\text{Cs}^+$  observed in our FM-AFM experiment, we evaluated the ground state energy differences among three systems shown in Figure A.6 using density functional theory. We considered montmorillonite systems based on our EDS measurement and FM-AFM observations (i.e., the system consists of  $\text{Cs}^+$  on the surface,  $\text{Al}^{3+}$  and  $\text{Mg}^{2+}$  in the octahedral sheet, and  $\text{Si}^{4+}$  in the tetrahedral sheet). The three different configurations are considered as shown in Figure A.1: (a) sparse configuration, (b) linear configuration in the [100] direction, and (c) linear configuration in the [120] direction. In all systems,  $\text{Mg}^{2+}$  and  $\text{Cs}^+$  ions are located near each other to minimize Coulomb energy by minimizing distance between positive and negative charges, whose origins are  $\text{Cs}^+$  and effective negative charge produced by the  $\text{Mg}^{2+}$  substitution in the octahedral sheet, respectively. For this purpose, we used the Vienna Ab Initio Simulation Package (VASP) [1-4], which is widely applied as a density functional theoretical code on the plane wave basis, supporting the projector argument wave method [5, 6] with periodic boundary conditions in three dimensions. Among exchange-correlation functional available in VASP, we used the Perdew–Burke–Ernzerhof functional [7]. The cut-off energy of the plan wave was 600 eV and  $1 \times 1 \times 1$  k-points were



employed in the calculations, and structural relaxation was repeated until the gradient forces on the atoms were less than 0.01 eV/Å. We made the systems from the bulk configuration based on the experimental result [8] by adding 10 Å vacant space in the c-direction, which is a sufficiently large distance allow the interaction between the surfaces to be neglected. The lattice parameters in these systems are shown in Table A.1.

We obtained the relative formation energy  $\Delta E$  shown in Table A.2. We set the highest formation energy obtained in the (c) system as zero energy, and  $\Delta E$  is defined as a relative energy difference from the energy. We found that the two systems with the linear configurations have almost same energy. The difference is only 3.69 kJ/mol for the unit cell shown in Fig. A.6. However, a large energy deviation (86.1 kJ/mol) was obtained between the (a) and (c) systems. We therefore conclude that the sparse configuration of the  $\text{Mg}^{2+}$  in the octahedral sheet is energetically favorable than the linear configurations. According to this result of simple calculation, it is indicated that the linear configurations of  $\text{Mg}^{2+}$  cannot be easily realized in the real system.

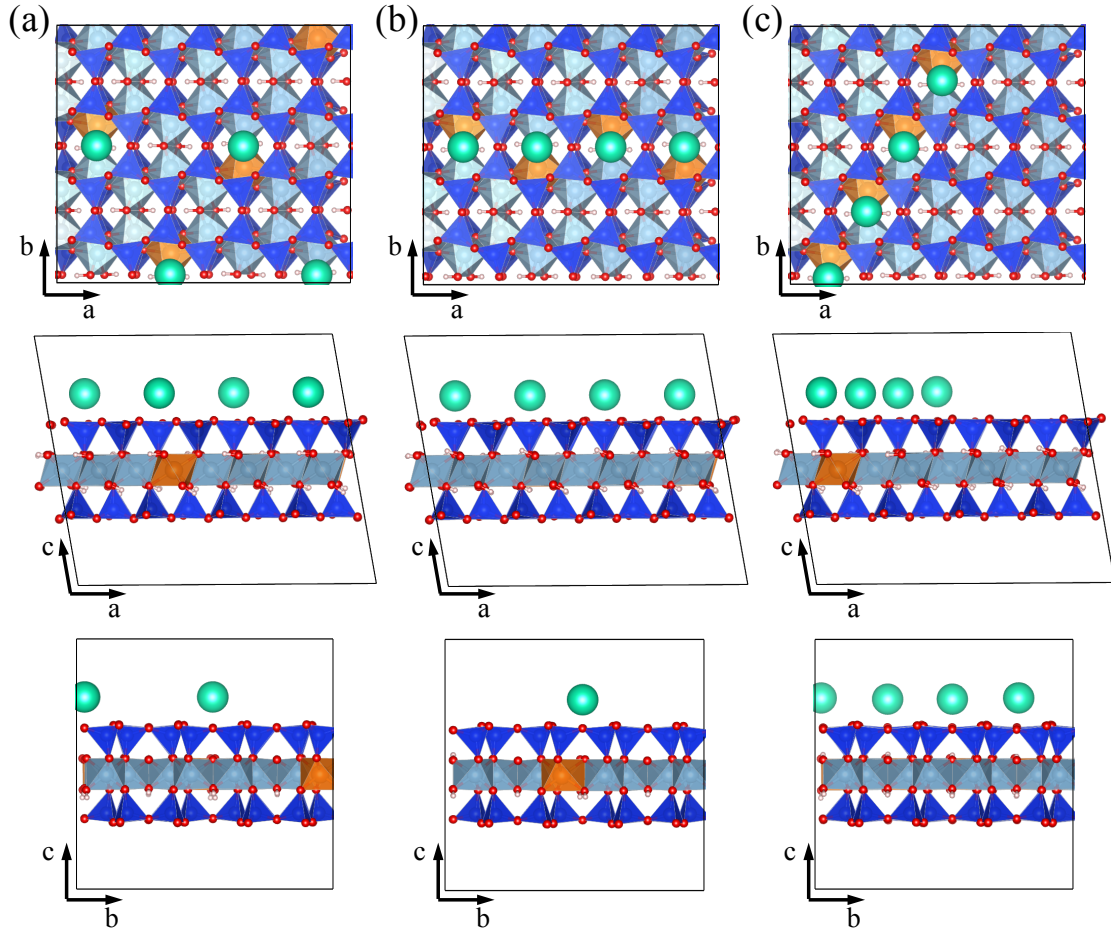


**Figure A.6.** Montmorillonite slab systems with (a) sparse configuration, (b) linear configuration in the [100] direction, and (c) linear configuration in the [120] direction of  $\text{Mg}^{2+}$  ions in the octahedral sheet and  $\text{Cs}^+$  on the surface. Blue tetrahedra and silver and orange octahedra represent polyhedra made by Si-O and Al-O and Mg-O, respectively. The green, red, and white spheres represent Cs, O, and H ions, respectively.

**Table A.1.** Lattice parameters

a [Å]	b [Å]	c [Å]	$\alpha$ [deg]	$\beta$ [deg]	$\gamma$ [deg]
20.72	17.89	17.62	90.00	99.62	90.00

**Table A.2.** Relative formation energy  $\Delta E$  [kJ/mol]

(a)	(b)	(c)
−86.1	−3.69	0

## Appendix References

- [1] Kresse, G. and Hafner, J., *Ab initio* molecular dynamics for liquid metals. *Phys. Rev. B* **47**, 558 (1993).
- [2] Kresse, G. and Hafner, J., *Ab initio* molecular-dynamics simulation of the liquid-metal-amorphous-semiconductor transition in germanium. *Phys. Rev. B* **49**, 14251 (1994).
- [3] Kresse, G. and Furthmüller, J., Efficiency of *ab-initio* total energy calculations for metals and semiconductors using a plane-wave basis set. *Comput. Mat. Sci.* **6**, 15-50 (1996).
- [4] Kresse, G. and Furthmüller, J., Efficient iterative schemes for *ab initio* total-energy calculations using a plane-wave basis set. *Phys. Rev. B* **54**, 11169 (1996).
- [5] Blöchl, P. E., Projector augmented-wave method. *Phys. Rev. B* **50**, 17953 (1994).
- [6] Kresse, G. and Joubert, D., From ultrasoft pseudopotentials to the projector augmented-wave method. *Phys. Rev.* **59**, 1758 (1999).
- [7] Perdew, J. P., Burke, K., and Ernzerhof, M., Generalized Gradient Approximation Made Simple. *Phys. Rev. Lett.* **77**, 3865 (1996).
- [8] Gournis, D., Lappas, A., Karakassides, M. A., Tobbens, D., Moukarika, A., A neutron diffraction study of alkali cation migration in montmorillonites. *Physics and Chemistry of Minerals* **35**, 49-58 (2008).